Biophysical Journal, Volume *114*

Supplemental Information

Measurement of Mesoscale Conformational Dynamics of Freely Diffusing Molecules with Tracking FCS

Charles Limouse, Jason C. Bell, Colin J. Fuller, Aaron F. Straight, and Hideo Mabuchi

Supplementary Materials and Methods

Single molecule tracking microscope: optics

The tFCS microscope was modified from our previously described tracking microscope [1] to increase the feedback bandwidth and permit fast electronic control of the position of both the tracking and probe beams, which is key for the internal dynamics measurements at sub-diffraction limit resolution. For real-time all-optical sensing of the position of the diffusing particle along the X and Y (transverse) axes, we used a 561 nm tracking laser (OBIS diode laser, Coherent Inc.) passing through two acousto-optic deflectors (AODs, 46080-2-LTD, Gooch and Housego) oriented to deflect the beam along the X and Y axes, respectively. The X and Y AODs were driven by 90° phase shifted sine waves so as to move the tracking laser beam around a circular orbit at 100 kHz and generate a particle-position dependent fluorescence modulation. To estimate the position of the particle axially (along the Z axis), we split the tracking laser into two paths corresponding to the s- and p-polarizations, and focused the two beams ∼1 µm to 2 µm apart in the sample. Each beam passed through a dedicated acousto-optic modulator (AOM-AF1 IntraAction) that we used as a fast shutter to rapidly (60 kHz) alternate excitation between the s and the p beams, and thereby dither the axial position of the tracking beam focus. The s and p paths were recombined before the X and Y AODs, so that both beams underwent the same rotation in the sample XY plane. To increase the tracking bandwidth and thereby improve the localization accuracy, this core design was updated for faster, photon-counting-limited feedback. The same AODs as the ones used to generate the tracking beam rotation also served as fast actuators allowing for fine adjustments of the beam transverse position with µs scale response time. The relay lenses between the active optical components (AODs) were placed in a 4-f configuration, as standard in confocal scanning systems. The tracking beam partially filled the microscope objective (Zeiss) back aperture to form a focus with a waist of ∼500-700 nm in the sample. The sample was mounted on a 3D piezo stage (Nano-PDQ, Mad City Labs). For the 657 nm probe beam,

we used a similar optical path with 2 AODs controlling the probe beam position, except that the beam was set-up to form a near diffraction-limited focus (∼320 nm waist) in the sample. The lateral offset between the probe and the tracking lasers was controlled electronically via the probe laser AODs. To facilitate the axial alignment between the tracking and probe beams, we used a tunable lens (el-10-30, Optotune), placed in the path of the probe beam in an infinity space of the microscope. The tunable lens provided us with an electronic knob used in the alignment stage, to easily displace the axial position of the probe beam focus in the sample and position it precisely at the tracking lock point. On the detection side, the fluorescence signal was first separated from the laser light by a dichroic mirror (Chroma ZT405/488/561/640rpc), and then a second dichroic (Chroma 625DCX) separated the probe (Atto647N or Alexa647) and reference (Cy3b) signals. In the reference path, we used a single avalanche photodiode (APD, Perkin-Elmer) to collect individual photons emitted by the Cy3b reference. To record photons from the probe dye, we used either a single APD, or two APDs arranged in a Hanbury Brown Twiss (HBT) configuration to eliminate detection dead time and after-pulsing effects from the fluorescence correlation data. Fluorescence filters were mounted directly in front the reference channel APD (Chroma ET595/50m) and the probe channel APD(s) (Chroma ET705/72m).

Single molecule tracking microscope: feedback

We achieved single-molecule tracking via an analog feedback loop with two feedback branches, which control respectively the position of the piezo stage (slow feedback branch, allowing long range tracking), as well as the position of the tracking laser via the AODs (fast, short range feedback branch). Briefly, the pulses generated by the APD in the reference channels were directly fed into both a dual phase lock-in amplifier (SR830, Stanford Research Systems) phase locked to the (100 kHz) XY rotation of the tracking laser, and into a single-phase lock-in amplifier (SR810, Stanford Research Systems) locked to the (60 kHz) axial dithering. The outputs of the lock-in amplifiers were used as X, Y and Z error signals (lock-in time

constant 30 µs for XY, 100 µs for Z) and fed back to the piezo stage driver (Nano Drive, Mad City Labs) via an integral controller. In parallel, the X and Y error signals were fed into a voltage controlled oscillator (VCO) driving the tracking AODs, after band-pass filtering (corner frequencies, 0.3 Hz and 100 Hz) and amplification. The amplification gain was tuned to obtain stable feedback. During tracking, we matched any displacement of the tracking beam with a similar displacement of the probe beam in such a way that both beams tracked the same site on the molecule. To do so, the feedback signal driving the tracking laser VCOs was also applied to the probe laser VCOs after amplification. To calibrate the amplification gain we applied a slow modulation (5 Hz) to the tracking and probe laser VCOs, and monitored the displacements of the beams on a CMOS camera (DCC1645C, Thorlabs). The camera was focused on the back surface of the sample coverslip to image the back reflection of the lasers. We chose a modulation drive that resulted in a ~ 2 µm amplitude modulation of the beam position, and adjusted the relative gain so that both beams followed the same trajectory.

Activation of feedback and fluorescence recording

During the experiments, the stage and the lasers were kept in idle position, but were automatically switched to tracking mode when individual molecules drifted into the confocal illumination volume. Such events were detected by a Schmitt trigger which activated the tracking feedback when the fluorescence of the probe dye was larger than 20-40 kPhotons/s. The feedback remained active until the reference dye bleached or the molecule escaped tracking. The fluorescence signals from the APDs in the reference and probe channels were recorded by a dual-channel time-interval analyzer board (GT653, GuideTech) operating in time-tagged mode, so that the arrival time of each photon was recorded for offline processing. Since we could record from only two APDs at once, the fluorescence signal from the reference dye was not recorded when the HBT configuration was used in the probe channel (the detector configuration used for each experiment is shown in **Table S2**). We will refer to the configuration

using a single probe APD as the reference-probe configuration (R-P configuration), and the HBT configuration as the probe-probe configuration (P-P configuration). The tracking laser power was monitored by a Si detector (PDA36A, Thorlabs) placed on a beam pick-off path, and recorded along with the piezo stage position (X, Y and Z channels), with a 10 kHz sampling rate (National Instruments).

Data preprocessing pipeline

To the tFCS signal of individual molecules, the fluorescence and tracking data that were recorded in continuous time were preprocessed by a custom pipeline written in Matlab (Mathworks) consisting of 6 steps, as detailed below.

Step 1: Isolation of individual molecules and fluorescence steps

Periods in the data where the microscope was either in active tracking mode or on standby were first isolated by applying a step detection algorithm to fit the Cy3b fluorescence signal with a piecewise constant signal. To detect abrupt changes, or steps, in the fluorescence mean, we used a simple top-down algorithm, which started with the assumption that there was no step in the fluorescence signal, and added steps one at a time, positioning the new step each time at the location that maximized the likelihood of the data. To decide whether to accept or reject the addition of the new step, we used an f-test to compare the residuals of the two nested models ($n+1$ steps vs n steps). If the p-value of the f-test was larger than a defined threshold, the algorithm stopped and the current segmentation was returned. We adjusted the threshold of the f-test empirically on a test data set, to obtain a qualitatively satisfactory segmentation of the fluorescence signal. The same threshold was used across the different samples to avoid sample bias. To compute the likelihood of the data, we assumed that in between each step, the fluorescence signal was constant with an additive Gaussian noise, where the variance of the noise was equal to the mean signal value (as would be expected for a Poisson emitter). Each interval obtained from the segmentation of the Cy3b

signal was further segmented by running the same step finder algorithm on the probe dye signal, in order to isolate sub-intervals where the probe dye was active and sub-intervals where the probe dye was in a dark state. For the experiments where we did not record the tracking dye signal (P-P detector configuration), we applied the segmentation algorithm directly to the probe dye signal of one of the two APDs in the probe channel.

Step 2: Classification of intervals

Segmented intervals were classified into three groups: 0, 1 and 2, representing periods of idle tracking, actively tracked molecules with bleached probe dye, and actively tracked molecules with active probe dye, respectively. To classify the intervals, we generated scatter plots of the probe fluorescence signal, the laser intensity, and either the reference dye fluorescence (R-P configuration) or the laser intensity variance (P-P configuration). The data typically clustered into three groups: low reference fluorescence or tracking laser variance and low probe fluorescence for group 0, high reference fluorescence or tracking laser variance and low probe fluorescence for group 1, high reference fluorescence or tracking laser variance and high probe fluorescence for group 2. Based on the scatter plots, we selected thresholds for the plotted variables that clearly separated the clusters. The thresholds were picked manually, which was the only non-fully automated step in the pipeline.

Step 3: Computation of the raw fluorescence correlation functions and intensities

When both the reference and probe signals were recorded (R-P detector configuration), we computed for each segmented fluorescence period a set of 3 correlation functions: the time auto-correlation of the signal from the reference channel APD $G_r(\tau)$, the auto-correlation of the signal from the probe channel APD $G_p(\tau)$, and the cross-correlation between these two signals $G_{r,p}(\tau)$. These three correlation functions were used to correct for the background signal and estimate the auto-correlation of the fluorescence signal originating from the probe dye only $g_p(\tau)$ (see Background correction section). When the probe signal was recorded from

two independent detectors (P-P detector configuration), we computed the cross-correlation between the signals from the two APDs in the probe channel $G_{p/p}(\tau)$. In both cases, the fluorescence correlation functions were computed directly from the time-tagged fluorescence data, consisting of the photon arrival times recorded by each APD, as described elsewhere [2]. The correlation functions were computed at ∼170 values of time-lags, logarithmically spaced between 1 µs and 1 s. For each detector, we also computed the average fluorescence intensity (I_r and I_p in the reference and probe channels, respectively, for the R-P configuration; $I_{p,\mathrm{APD1}}$ and $I_{p,\mathrm{APD2}}$ for the P-P configuration) by dividing the number of photons by the interval duration.

Step 4: Background correction

We modeled the time-dependent signal in the probe channel $I_p(t)$ as the sum of the fluorescence of the probe dye $i_p(t)$, and of a background noise $i_B(t)$. We modeled the background process $i_B(t)$ as the sum of a time-independent Poissonian noise $i_{b,p}$ (which encompasses detector dark noise and scattering from the buffer and the microscope optics), and of a time-dependent crosstalk (or leakage) from the reference dye into the probe channel $i_l(t)$. Likewise, in the reference channel, the measured intensity $I_r(t)$ was modeled as the sum of the fluorescence signal from the reference dye $i_r(t)$ and a background noise $i_{b,r}$. When the crosstalk of the reference dye into the probe channel is negligible, then the measured correlation function in the probe channel $G_p(\tau)$ relates to the true correlation of the probe dye fluorescence (after background correction) $g_p(\tau)$ by an overall time-lag independent rescaling:

$$g_p(\tau) = \frac{1}{\theta_p^2} G_p(\tau) \tag{1}$$

where the background correction factor p is defined as

$$\theta_p = \frac{i_p}{I_p} \tag{2}$$

and where i_p and I_p designate the mean values of $i_p(t)$ and $I_p(t)$, respectively. When the leakage of reference dye into the probe channel is not negligible, the relationship between $G_p(\tau)$ and $g_p(\tau)$ takes a more complicated, time-lag dependent form. In that case, we derived the following expression (SI Appendix):

$$g_p(\tau) = \frac{1}{\theta_p^2} G_p(\tau) + \frac{\theta_l^2(\theta_p - 1)^2}{\theta_p^2 \theta_r^2} G_r(\tau) + \frac{2\theta_l(\theta_p - 1)}{\theta_p^2 \theta_r} G_{r,p}(\tau) \tag{3}$$

where

$$\theta_r = \frac{i_r}{I_r} \qquad \theta_l = \frac{i_l}{i_B} \tag{4}$$

However, we found that the second and third terms in the sum (3) are typically small, and we therefore neglected these terms when data were taken with the P-P configuration of the detectors.

Step 5: Background estimation

To apply the background correction (3, 4), we need to estimate the signal to noise factors θ_r, θ_p and θ_l. This amounts to estimating the mean background scattering intensities $i_{b,r}$, i_b, and the leakage intensity i_l, which may vary from molecule to molecule due to variations in tracking laser power. $i_{b,r}$ and $i_{b,p}$ were first estimated either by doing a blank measurement consisting of recording the fluorescence signal from the buffer in absence of labeled molecules at different tracking laser powers, or equivalently by looking at the intervals in the tFCS data classified in group 0 (**Fig. S1**). For both approaches, we linearly fit the mean noise intensity $i_{b,r/p}$ as a function of the tracking laser power P_{track} to obtain the background scattering coefficients $\alpha_{b,r/p}$ and $\alpha_{b,r/p}$ defined as the coefficients of the linear regression:

$$i_{b,r/p} = \alpha_{b,r/p} P_{\text{track}} + \beta_{b,r/p} \tag{5}$$

To obtain the mean leakage noise, we used the intervals in the data classified in group 1, corresponding to molecules with an active reference dye and bleached probe dye. We estimated the leakage coefficient α as

$$\alpha = \frac{i_l}{i_r} = \frac{\langle I_p - \alpha_{b,p} P_{\text{track}} - \beta_{b,p} \rangle_1}{\langle I_r - \alpha_{b,r} P_{\text{track}} - \beta_{b,r} \rangle_1} \tag{6}$$

where $\langle \rangle_1$ designates the average over molecules in group 1.

Step 6: Optional removal of outliers

For the samples that were expected to be homogeneous (for instance the DNA samples in the end-to-end dynamics measurements) we removed outliers that exhibited a fluorescence correlation function $g_p(\tau)$ distinctively different from the rest of the population. This was achieved by computing for each molecule in group 2 a total variation score calculated as the integral of $g_p(\tau)$ between 1 s and 1 ms, and discarding molecules with a total variation score more that 5 median absolute deviation (MAD) away from the population median.

Estimation of diffusion coefficients

The diffusion coefficient of each molecule was estimated from its trajectory as previously described [3]. Briefly, we computed the mean square displacement of the stage along each axis as a function of the time increment τ, and re-scaled it by dividing by 2τ. The obtained quantity $\hat{D}(\tau)$ provides an estimator of the diffusion coefficient as the function of the time increment, which was fit with a parametric model including the molecule diffusion and the response of the feedback system to obtain the diffusion coefficient of the molecule [3].

Estimation of molecular macrostate in the LacI experiments

In the LacI experiments, we used a clustering algorithm to classify each molecule shown in **Fig. 5B, C, D** as well as the 100 ms subtraces of the molecules shown in **Fig. 5E** as

open, looped or lassoed. Clustering was done based on $g_p(\tau)$, using either a two- (lasso and looping construct) or three-components (3 sites construct and 100 ms subtraces) Gaussian Mixture model, representing the distribution of compaction scores and correlation function amplitude (average value of $g_p(\tau)$ between 1-10 μs).

Simulations

For the numerical simulations (**Fig. 2, S4, S5**), we modeled the intramolecular dynamics between the reference and the probe dye as an isotropic 3-dimensional Ornstein-Uhlenbeck (O.U.) process (i.e., the time-autocorrelation of the reference-to-probe dye vector projected along any axis $\sigma rp(\tau)$ is a mono-exponential relaxation $\sigma rp(\tau) = \frac{1}{\sqrt{3}}\sigma_{rp}(0)e^{-\tau/\tau_c}$, where $\sigma_{rp}(0)$ is the RMS amplitude of the reference-to-prove dye motion). We chose a relaxation timescale of $\tau_c = 10\,\text{ms}$ or $\tau_c = 1\,\text{ms}$. To account for localization error during feedback, we modeled the motion of the reference dye with respect to the tracking lock-point as a second, independent O.U. process with a 1 ms relaxation timescale, chosen to match our 1 kHz feedback bandwidth, and an RMS amplitude along each axis of 0, 50 or 100 nm. For each set of parameters, we simulated 20 fluorescence traces of 5 s each. To do so, we first simulated the two O.U. processes using a 1 µs simulation step size to obtain the trajectory of the probe dye position x_p^t with respect to the tracking center. To obtain the probe fluorescence signal, we simulated an inhomogeneous Poisson process with a time-variable instantaneous rate given by

$$i_p(t) = A\Phi\left(x_{\text{err}}^t + x_{r-p}^t - d_{t-p}\right) \tag{7}$$

where d_{t-p} is the tracking-to-probe beam offset, $\Phi(x)$ is the intensity profile of a Gaussian beam with $w(x_z) = w_0\left(1 + \left(\frac{x_z\lambda}{\pi w_0}\right)^2\right)^{1/2}$ describing the axial evolution of the beam waist. The prefactor A was chosen to get an average fluorescence rate of 10^5 photons/s, which is routinely obtained from molecules labeled with a single Atto647N dye (**Table S2**). The Poisson process was simulated using the thinning method [4]. Background scattering noise

was simulated separately as an independent Poisson process with a homogeneous rate of 10^4 photons/s, chosen to match the signal-to-noise value of S/N=10 typically observed in our experiments (**Fig. S1**), and added to the probe dye signal. We assessed the resolvability of the intramolecular motion as a function of the reference-to-probe RMS distance by comparing the amplitude of the tFCS signal at short time lags, for which the correlation function has plateaued (either $g_p(\tau = 10\,\mu s)$ or $g_p(\tau = 1\,\mu s)$ for $\tau_c = 10\,ms$ and $1\,ms$, respectively) between molecules with a given reference-to-probe RMS distance and control molecules where the probe and reference dyes were co-localized (10 molecules per group, t-test).

DNA preparation and labeling

Each DNA fragment for the DNA dynamics experiment was obtained by digestion of a plasmid with XbaI and EcoRI, followed by gel electrophoresis and gel purification. The plasmids were randomly selected from our database and then screened for their XbaI-EcoRI digestion pattern so as to produce fragments of the desired lengths. The DNA used for the nucleosome arrays assembly was purified by XbaI and EcoRI digestion of a puc18 plasmid containing 19 repeats of the 601 nucleosome positioning sequence, and was the same as the 3.9 kb molecule in **Fig. 3**. To label these molecules, short dsDNAs were prepared by annealing two or three short oligonucleotides, each harboring a specific functionality (XbaI or EcoRI 5'' end, Cy3b, Atto647N, or Alexa647 modification), so as to produce appropriate overhangs and fluorescent tags to ligate on the ends of the XbaI-EcoRI fragment for SE or OE labeling (**Table S1**). Ligation was performed by incubation with T4 ligase for 30 min and the ligation products were gel purified. Unmodified oligonucleotides were purchased as used (Integrated DNA Technologies, IDT). Fluorescently labeled oligonucleotides were prepared by conjugation of NHS-Ester reactive dyes (Monoreactive NHS-Ester Cy3b from GE Healthcare, NHS-Ester Atto647N from Sigma, Alexa647 from Invitrogen) to amine-modified oligonucleotides (IDT), followed by PAGE purification.

To prepare DNA constructs containing the LacO sites at desired positions, we designed

a GeneBlock (IDT) sequence with two LacO sites separated by ∼300 bp which we modified using conventional cloning techniques, to adjust the distance between the two LacO sites, replace the desired LacO sites with shuffled sequences or other LacO variants (LacOsym), or insert a third LacO site in the middle of the construct. Fluorescent labeling of the constructs with Cy3b on one end and Atto647N on the other end was done by PCR amplification with fluorescently labeled primers, followed by gel purification (**Table S1**).

LacI purification

LacI was endogenously expressed from the E. coli BLIM strain (Addgene #35609) transformed with plasmid pLS1 (Addgene #31490). Cultures were grown in 2xYT with 100 ug/mL carbenicillen overnight, and cells were harvested by centrifugation at 4000 x g for 10 minutes. ∼36 g of wet cell paste was dounced in 120 mL of Buffer BB (200 mM TrisHCl pH 7.6, 200 mM KCl, 10 mM MgOAc, 2 mM DTT, 5% glucose, 1 mM PMSF and 0.25 mg/mL lysozyme) then flash frozen and stored at -20 C. Phosphocellulose was prepared by swelling 20 g of phosphocellulose in 1 L of water, then decanted. This process was repeated (in 1L volumes): 3X water, 4X 0.5 N NaOH, 1X water, 4X 0.5 N HCl, 1X water, and 2X 0.2 M KHPO4 (pH 7.6). The slurry was transferred to a Buchner funnel with a porous ceramic filter and washed with 0.2 M KHPO4 (pH 7.6). The slurry was then poured into a column packed by gravity flow with a final bed volume of ∼120 mL. The frozen cell slurry was thawed at 4C and stirred in a beaker for 20-30 minutes. The lysate was then treated with 2 mg of DNase and stirred for 5-10 minutes. The lysate was dounced, then centrifuged at 12k rpm in a JA 20 rotor for 40 minutes. The supernatant was transferred to a beaker, and ammonium sulfate was slowly added while stirring to a final concentration of 23.1 g AmSO4 per 100 mL lysate. The precipitated lysate was centrifuged for 10 minutes at 4000 x g, and the pellet was resuspended in Buffer BB plus 23.1 g/mL AmSO4, dounced and centrifuged again. The pellet was then resuspended in 40 mL of Buffer A (45 mM KHPO4 (pH 7.6), 5% glucose and 1 mM DTT) and then dialyzed overnight against 2L of the same buffer. The lysate was

centrifuged at 4000 g for 15 minutes to remove insoluble material, and then loaded onto the phosophocellulose column equilibrated in Buffer A. After the lysate was loaded, the column was washed with Buffer A until the UV absorbance returned to baseline. A linear gradient was run over 120 minutes with a flow rate of 0.8 mL/mL from Buffer A to Buffer B (300 mM KHPO4 (pH 7.6), 5% glucose and 1 mM DTT). Fractions were collected and UV absorbance was monitored. The major peak fractions (∼38 mL) were pooled containing ∼50 mg of >90% pure LacI, which was then concentrated via precipitation by adding 8.8 g AmSO4, centrifuging at 8000 rpm in a JA 20 rotor for 20 minutes. The LacI pellet was resuspended in 4.5 mL Buffer B, and injected into a S200 HiLoad 16/60 size exclusion column equilibrated with Buffer B. ∼10% of the input protein eluted in the void volume and was discarded, with the remaining protein eluting as a homogeneous peak consistent with the column mobility of a tetramer. Peak containing fractions were pooled and flash frozen. The concentration was determined using an extinction coefficient of $22\,450\,\mathrm{M}^{-1}\,\mathrm{cm}^{-1}$ (monomer) and determined to be free of DNA contamination (260/280 ratio = 0.45).

Nucleosome arrays reconstitution

To reconstitute nucleosome arrays [5], we prepared individual 20 µL assembly mixes each containing unlabeled 19x601 DNA (19-mer tandem array of the 601 positioning sequence) at a concentration of 1.5 µM of 601 monomers, dual-labeled 19x601 DNA (with a single Cy3b and a single Atto647N placed either on the same end or on opposite ends of the DNA) at 150 nM of 601 monomers and variable amounts of purified H3/H4/H2A/H2B octamers in high salt buffer (HSB: 10 mM Tris pH 7.4, 0.1 mM EDTA, 2M NaCl). Unlabeled DNA was used in addition to labeled DNA at a 10:1 ratio to increase the overall array concentration during tFCS and thus minimize histone dissociation, while maintaining the concentration of labeled molecules at $\sim$ 1 pM). Additionally, a 0.5x excess of H2A/H2B dimers per 601 monomer was added to each assembly to increase the array stability against dimer exchange. We used individual mixes to titrate the stoichiometric ratio of octamers from 0.4 to 1.4 per

601 site. Each assembly mix was loaded into a 20 µL dialysis button (Hampton Research) sealed with a 3.5 kDa MWCO dialysis membrane (Spectrum Labs). The buttons were plunged into 500 mL of HSB, which was slowly exchanged using a system of peristaltic pumps against 2 L of low salt buffer (LSB: 10 mM Tris pH 7.4, 0.1 mM EDTA, 10 mM NaCl), over 36 hours (0.5 mL/minute). The quality of each array assembly was assessed by AvaI restriction digest (overnight incubation at room temperature) followed by native-PAGE electrophoresis [5]. AvaI cuts in between each monomeric repeat of the positioning sequence and allows us to determine the histone saturation ratio (average fraction of 601 sites occupied by a histone octamer).

Appendix: Mathematical derivations

Background correction of fluorescence correlation functions

We model the signal in the reference channel I_r^t (where the exponent t indicates the time dependency of the signal) as the sum of the fluorescence signal from the reference dye i_r^t and a constant background scattering $i_{b,r}$. The signals I_r^t and i_r^t refer to the instantaneous photon emission rates, and are stochastic processes driven by the random trajectory of the probe dye within the probe beam. In the probe channel, we model the measured signal I_p^t as the sum of the probe dye fluorescence signal i_p^t, a constant background scattering $i_{b,p}$, and a leakage intensity $i_l^t = \alpha i_r^t$, where α is the leakage coefficient accounting for the fluorescence crosstalk between the reference and probe channels.

The measured instantaneous intensities in the reference and probe channels are therefore:

$$I_r^t = i_r^t + i_{b,r} \tag{8}$$

$$I_p^t = i_p^t + i_B^t \tag{9}$$

where the total background in the probe channel is

$$i_B^t = \alpha i_r^t + i_{b,p} \tag{10}$$

We define the signal-to-noise ratios

$$\theta_r = \frac{i_r}{I_r} \qquad \theta_p = \frac{i_p}{I_p} \qquad \theta_l = \frac{i_B - i_{b,p}}{i_B} \tag{11}$$

where we dropped the t subscript to indicate time-averaged intensities.

The cross-correlation between two generic stationary stochastic signals a^t and b^t with mean values a and b is defined as

$$g[a,b](\tau) = \frac{\mathbb{E}\left[a^t b^{t+\tau}\right]}{\mathbb{E}\left[a^t\right]\mathbb{E}\left[b^t\right]} - 1 \tag{12}$$

$$= \frac{\mathbb{E}\left[a^t b^{t+\tau}\right]}{ab} - 1 \tag{13}$$

and the auto-correlation of a^t is simply denoted

$$g[a](\tau) = \frac{\mathbb{E}\left[a^t a^{t+\tau}\right]}{a^2} - 1 \tag{14}$$

To express the auto-correlations of the reference and probe dye fluorescence intensities $g_r(\tau)$ and $g_p(\tau)$ (as a short-hand notation for $g[i_r](\tau)$ and $g[i_p](\tau)$) and their cross-correlation $g_{r,p}(\tau)$ (as a short-hand notation for $g[i_r, i_t](\tau)$), as a function of the auto-correlations and the cross-correlations of the measured signals $G_r(\tau)$, $G_p(\tau)$ and $G_{r,p}(\tau)$ (as a short-hand notation for $g[I_r](\tau)$, $g[I_p](\tau)$ and $g[I_r, I_p](\tau)$, respectively), we use Eq. 8 and the following algebraic relationship on correlation functions, which is valid for any stochastic stationary

signal a_t, b_t, c_t, d_t :

$$g[a+b, c+d] = \frac{a}{a+b}\frac{c}{c+d}g[a,c] + \frac{a}{a+b}\frac{d}{c+d}g[a,d] + \frac{b}{a+b}\frac{c}{c+d}g[b,c] + \frac{b}{a+b}\frac{d}{c+d}g[b,d] \tag{15}$$

We find that the measured ($G(\tau)$) and background-corrected ($g(\tau)$) correlation functions are related by the linear transformation:

$$\begin{bmatrix} G_r \\ G_p \\ G_{r,p} \end{bmatrix} = \begin{bmatrix} \theta_r^2 & 0 & 0 \\ (1-\theta_p)^2\theta_l^2 & \theta_p^2 & 2\theta_p(1-\theta_p)\theta_l \\ \theta_r(1-\theta_p)\theta_l & 0 & \theta_r\theta_p \end{bmatrix} \begin{bmatrix} g_r \\ g_p \\ g_{r,p} \end{bmatrix} \tag{16}$$

This derivation uses the fact that the scattering background $i_{b,p}$ (resp. $i_{b,r}$) and the fluorescence signal i_p^t (resp. i_r^t) in the probe (resp. reference) channel are statistically independent, so the cross-correlation between these two processes vanishes.

We can finally invert this relation to get:

$$\begin{bmatrix} g_r \\ g_p \\ g_{r,p} \end{bmatrix} = M \begin{bmatrix} G_r \\ G_p \\ G_{r,p} \end{bmatrix} \tag{17}$$

where

$$M = \begin{bmatrix} \frac{1}{\theta_r^2} & 0 & 0 \\ \frac{\theta_l^2(\theta_p-1)^2}{\theta_p^2\theta_r^2} & \frac{1}{\theta_p^2} & \frac{2\theta_l(\theta_p-1)}{\theta_p^2\theta_r} \\ \frac{\theta_l(\theta_p-1)}{\theta_p\theta_r^2} & 0 & \frac{1}{\theta_p\theta_r} \end{bmatrix} \tag{18}$$

which shows that we can obtain the background corrected correlation function of the probe dye signal $g_p(\tau)$ from the measured auto-correlations of the signals recorded in the probe and reference channels and their cross-correlation.

Relationship between the fluorescence correlation signal in tFCS and the motion of the probe dye

In this section, we describe the mathematical formalism necessary to analyze the tFCS signals. We describe some assumptions which allow us to obtain a tractable form for the fluorescence correlation function $g_p(\tau)$, which is useful to gain insight into the relationship between the intramolecular dynamics and the fluorescence correlation signal.

General expression of the fluorescence correlation signal in tFCS

In absence of dye blinking, the probe fluorescence is described by a Poisson process with time-varying intensity i_p^t

$$i_p^t = P\eta\phi(x_p^t - d) \tag{19}$$

where P is the laser power, η is the quantum yield of the dye, $\phi(x)$ is the spatial distribution of the probe beam intensity, x_p^t is the position of the probe dye (vector of dimension 3 representing the x,y and z coordinates with respect to the center of the tracking beam), and d is the offset vector between the tracking and probe beams. To account for the photophysics of the dye, we describe the dye intrinsic dynamics with a stochastic process D^t.

An important assumption is that the dye dynamics is independent of the motion of the dye in the beam. Under this assumption, the fluorescence intensity from the probe can be written as

$$\tilde{i}_p^t = D^t i_p^t \tag{20}$$

and the fluorescence autocorrelation of the probe dye fluorescence is, using the notations defined in Eq. 12

$$g[\tilde{i}_p](\tau) = -1 + (1 + g[D](\tau))\,(1 + g[i_p](\tau)) \tag{21}$$

Therefore, given the illumination profile $\phi(x)$, if one has a parametric model for the blinking dynamics of the dye D^t and for the statistics of the probe dye motion x_p^t, one can use Eqs.

19 and 21 to derive an expression for the fluorescence autocorrelation and use parametric estimation techniques to fit the experimental correlation data. In the next section, we show that if the probe dye motion x_p^t satisfies some conditions, then an analytical expression can be derived for $g[i_p]$.

Simplified form of the fluorescence correlation signal in tFCS in the case of a Gaussian process

The fluorescence correlation function of an individual molecule in tFCS under these conditions was derived previously [6]. Here, we derive the expression of the fluorescence correlation in the case of a variable offset between the tracking and probe beams. We show that the amplitude of the fluorescence correlation function has, upon renormalization, a quadratic dependency in the value of the tracking-to-probe beam offset. To derive an analytic expression for $g[i_p]$, we make the following assumptions:

1. The intensity profile of the probe beam is described by a 3-dimensional Gaussian: $\phi(x) = e^{-2w^{-T}xw^{-1}}$ where w is a 3x3 diagonal matrix with the beam waist along the three axes (w_x, w_y and w_z) as entries.

2. The process x_p^t is a stationary Gaussian process, in the sense where it is fully described by its second order statistics (for a more precise definition, see [7]).

$$\sigma_p(\tau) = \mathbb{E}\left[x_p^t (x_p^{t+\tau})^T\right] \tag{22}$$

3. The blinking dynamics of the probe dye is independent of the tracking-to-probe beam offset d.

Under these assumptions, the fluorescence correlation function can be computed analytically. We first normalize all of the length variables with respect to the beam dimensions by defining:

$$X_p^t = 2w^{-1}x_p^t \quad , \quad \delta = 2w^{-1}d \tag{23}$$

For computational purposes, we also define the two-timepoint vectors Y and Δ (expressed in block matrix notations):

$$Y = \begin{bmatrix} X_p^t \\ X_p^{t+\tau} \end{bmatrix} \qquad \Delta = \begin{bmatrix} \delta \\ \delta \end{bmatrix} \tag{24}$$

Under assumption 2, the statistics of Y are entirely defined by the covariance matrix

$$\Sigma(\tau) = \mathbb{E}\left[YY^T\right] \tag{25}$$

which itself relates to the covariance matrix of the probe dye motion $\sigma_p(\tau)$ (Eq. 22) by the expression (in block matrix notation)

$$\Sigma(\tau) = 4W^{-1} \begin{bmatrix} \sigma_p(0) & \sigma_p(\tau) \\ \sigma_p(\tau) & \sigma_p(0) \end{bmatrix} W^{-1} \tag{26}$$

where

$$W = \begin{bmatrix} w & 0 \\ 0 & w \end{bmatrix} \tag{27}$$

(W is a 6x6 matrix, written above in block notations). By writing

$$i_p(t)i_p(t+\tau) = e^{-\frac{1}{2}(Y-\Delta)^T(Y-\Delta)}$$

and by using the probability density for a Gaussian process

$$\mathbb{P}[\phi(Y) = y] = \frac{1}{\sqrt{(2\pi)^6 \det(\Sigma)}} e^{-\frac{1}{2}(y-\Delta)^T\Sigma^{-1}(y-\Delta)} \tag{28}$$

we obtain the autocorrelation of the intensity :

$$\mathbb{E}\left[i_p(t)i_p(t+\tau)\right] = \frac{1}{\sqrt{\det(\mathbf{1}+\Sigma)}} e^{-\frac{1}{2}\Delta^T\left(\mathbf{1}-\Sigma(\mathbf{1}+\Sigma)^{-1}\right)\Delta} \tag{29}$$

Likewise, the expectation value for the intensity is

$$\mathbb{E}\left[i_p(t)\right]\mathbb{E}\left[i_p(t+\tau)\right] = \frac{1}{\sqrt{\det(\mathbf{1}+\Sigma_\infty)}} e^{-\frac{1}{2}\Delta^T\left(\mathbf{1}-\Sigma_\infty(\mathbf{1}+\Sigma_\infty)^{-1}\right)\Delta} \tag{30}$$

where

$$\Sigma_\infty = 4W^{-1}\begin{bmatrix}\sigma(0) & 0\\ 0 & \sigma(0)\end{bmatrix}W^{-1} \tag{31}$$

We finally get the expression for the fluorescence correlation function

$$g[i_p](\tau) = \frac{\sqrt{\det(\mathbf{1}+\Sigma_\infty)}}{\sqrt{\det(\mathbf{1}+\Sigma)}} e^{-\frac{1}{2}\Delta^T\left(\Sigma_\infty(\mathbf{1}+\Sigma_\infty)^{-1}-\Sigma(\mathbf{1}+\Sigma)^{-1}\right)\Delta} - 1 \tag{32}$$

This expression assumes that the coordinate system is such that $E[x_p^t] = 0$, which can always be obtained modulo a redefinition of the tracking-to-probe-beam offset d.

Fluorescence correlation signal in tFCS for an isotropic process with independent axes

Under the assumption that the motion is isotropic and there is no cross-correlation between the x, y, z axes (this excludes a rigid body rotation, because in that case the motion along the 3 axes is correlated), we can further simplify Eq. 32. The process $x_p(t)$ is then fully characterized by the length correlation (in space units) $s_0 s(\tau) = \mathbf{E}\left[x_p(t)^T x_p(t+\tau)\right]$ where $s(\tau)$ is normalized so that $s(0) = 1$, and we can write Σ as

$$\Sigma = s_0 W^{-2} + s_0 s(\tau) W^{-1} K W^{-1} \tag{33}$$

where

$$K = \begin{pmatrix} 0 & \mathbf{1}_3 \\ \mathbf{1}_3 & 0 \end{pmatrix} \tag{34}$$

If we assume that the illumination is isotropic along the x and y axis, we can define $w_{\parallel} = w_x = w_y =$ and $\epsilon = \frac{w_{\parallel}}{w_z}$. Then we obtain

$$1 + g_p(\tau) = \frac{(1+v)^2}{(1+v+s(\tau)v)(1+v-s(\tau)v)} \frac{1+\epsilon v}{\sqrt{(1+\epsilon v+s(\tau)\epsilon v)(1+\epsilon v-s(\tau)\epsilon v)}} \exp\left(\frac{d_{\parallel}^2 s(\tau) v}{(1+v)(1+v+s(\tau)v)} + \frac{\epsilon^2 d_{\perp}^2 s(\tau)\epsilon v}{(1+\epsilon v)(1+\epsilon v+\epsilon s(\tau)v)}\right) \tag{35}$$

where $v = \frac{4}{3} s_0 / w_{\parallel}^2$ is the mean square amplitude of the probe motion normalized with respect to the beam size. Note that in the case where the probe dye motion is described by an Ornstein-Uhlenbeck process with relaxation timescale τ_c, as it is the case in our simulations (**Fig. 2, S5, S7**), the normalized length cross-correlation is $s(\tau) = e^{-\tau/\tau_c}$.

Effect of the tracking localization error

The presence of tracking error is straightforward to take into account. Denoting x_r^t the position of the reference dye with respect to the center of the tracking beam rotation, we can express the probe dye position x_p^t as the sum of a vector describing the intramolecular dynamics $x_{\text{r-p}}^t = x_p^t - x_r^t$ (i.e. the reference-to-probe dye dynamics) and of a vector describing the tracking error $x_{\text{err}}^t = x_r^t$ (which is equal to zero in the case of perfect tracking),

$$x_p^t = x_{\text{r-p}}^t + x_{\text{err}}^t \tag{36}$$

Since the molecular dynamics and the tracking error are statistically independent, the covariance matrix has the form

$$\Sigma(\tau) = \Sigma_{\text{r-p}}(\tau) + \Sigma_{\text{err}}(\tau) \tag{37}$$

and the correlation function is now, using Eq. 32

$$g[i_p](\tau) = -\mathbf{1} + \sqrt{\frac{\det\left(\mathbf{1} + \Sigma_{\text{r-p},\infty} + \Sigma_{\text{err},\infty}\right)}{\det\left(\mathbf{1} + \Sigma_{\text{r-p}} + \Sigma_{\text{err}}\right)}} \\ e^{-\frac{1}{2}\Delta^T\left((\Sigma_{\text{r-p},\infty}+\Sigma_{\text{err},\infty})(\mathbf{1}+(\Sigma_{\text{r-p},\infty}+\Sigma_{\text{err},\infty}))^{-1}-(\Sigma_{\text{r-p}}+\Sigma_{\text{err}})(\mathbf{1}+(\Sigma_{\text{r-p}}+\Sigma_{\text{err}}))^{-1}\right)\Delta} - 1 \quad (38)$$

Note that the contributions from the tracking error and the end-to-end motion do not factorize, and we cannot write the correlation function as a product of an internal dynamics part and a tracking error part.

Relative correlation function

In order to compare the fluorescence correlation functions in the centered- and side-illumination conditions, we define the relative fluorescence correlation function as:

$$g_{\text{rel}}[\tilde{i}_b](\tau) = \ln\left(1 + g[\tilde{i}_p](\tau, \delta = \delta_1 c)\right) \quad (39)$$

$$- \ln\left(1 + g[\tilde{i}_p](\tau, \delta = \delta_2 c)\right) \quad (40)$$

$$= g_{\text{rel}}[D](\tau) + g_{\text{rel}}[i_p](\tau) \quad (41)$$

where c is the unit vector along which the probe beam is being displaced with respect to the tracking beam, δ_1 and δ_2 are scalar values of the offset in the centered- and side-illumination condition, respectively (typically $\delta_1 = 0$). We also define the relative intensity:

$$\tilde{i}_{\text{rel}} = 2\ln\left(\frac{\tilde{i}_b[\delta = \delta_1 c]}{\tilde{i}_b[\delta = \delta_2 c]}\right) \quad (42)$$

Under assumption 3, the term corresponding to the dye dynamics $g_{\text{rel}}[D]$ in Eq. 41 vanishes and we obtain

$$g_{\text{rel}}[\tilde{i}_b](\tau) = (\delta_2^2 - \delta_1^2)\frac{1}{2}C^T\left(\Sigma_\infty(\mathbf{1} + \Sigma_\infty)^{-1} - \Sigma(\mathbf{1} + \Sigma)^{-1}\right)C \quad (43)$$

where $C = \begin{bmatrix} c \\ c \end{bmatrix}$. Likewise, the relative intensity becomes

$$i_{\mathrm{rel}} = (\delta_2^2 - \delta_1^2)\frac{1}{2} C^T \left(\mathbf{1} - \Sigma_\infty (\mathbf{1} + \Sigma_\infty)^{-1} \right) C \tag{44}$$

This expression shows that the relative correlation function and the relative intensity have a quadratic dependency in the offset amplitude δ_2, which we verified experimentally in **Fig. S8**.

References

[1] McHale, K., Berglund, A. J. & Mabuchi, H. Quantum dot photon statistics measured by three-dimensional particle tracking. *Nano letters* **7**, 3535–9 (2007).

[2] Laurence, T. A., Fore, S. & Huser, T. Fast, flexible algorithm for calculating photon correlations. *Optics letters* **31**, 829–31 (2006).

[3] McHale, K. & Mabuchi, H. Precise characterization of the conformation fluctuations of freely diffusing DNA: beyond Rouse and Zimm. *Journal of the American Chemical Society* **131**, 17901–7 (2009).

[4] Lewis, P. A. W. & Shedler, G. S. Simulation of nonhomogenous Poisson processes by thinning. *Naval Research Logistic Quarterly* **26**, 403–414 (1979).

[5] Guse, A., Fuller, C. J. & Straight, A. F. A cell-free system for functional centromere and kinetochore assembly. *Nature protocols* **7**, 1847–69 (2012).

[6] McHale, K. & Mabuchi, H. Intramolecular fluorescence correlation spectroscopy in a feedback tracking microscope. *Biophysical journal* **99**, 313–22 (2010).

[7] MacKay, D. J. C. *Information theory, inference and learning algorithms. Cambridge University Press* (2003).

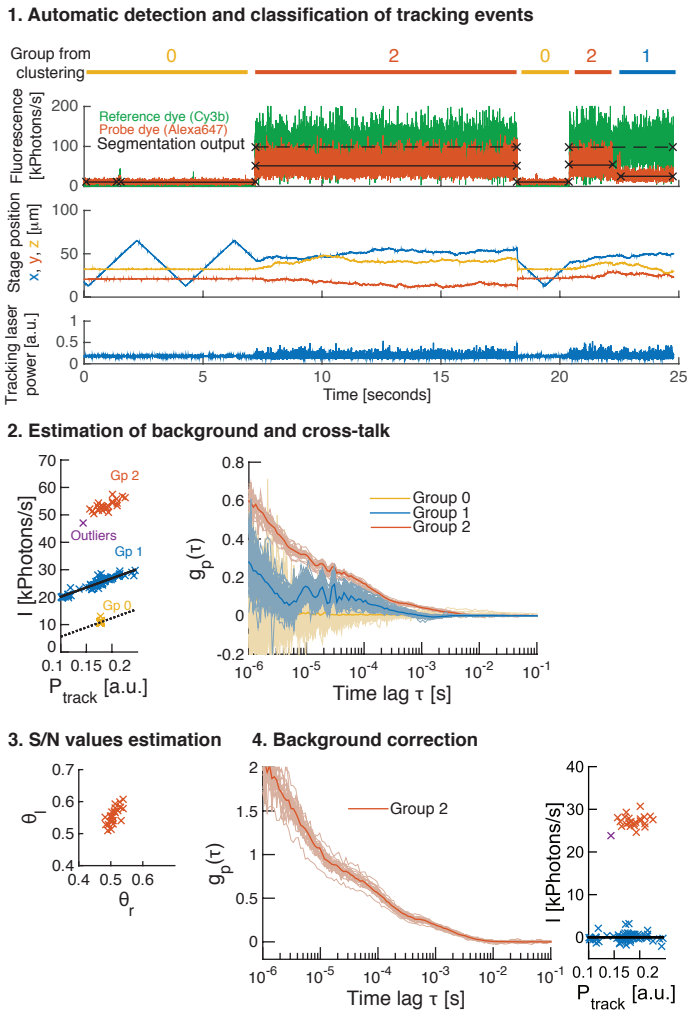

Figure S1. Data pre-processing pipeline: detection of individual molecules and background correction All data shown are from the 3.8 kbp OE DNA molecules (**Fig.** 3) and were recorded using the side-illumination.

Step 1*: Detection and classification of time intervals in the recorded data corresponding to individual molecules.* Typical time course of the probe fluorescence signal (top plot, binned at 3 ms for visualization), the microscope stage position (middle plot), and the tracking laser power (bottom plot) during a tFCS experiment. Individual molecules spontaneously drift in the confocal detection volume (e.g.: $t = 7 - 17$ s) and trigger activation of the feedback loop. This is observed in the abrupt change in laser power, which is adjusted in real-time to maintain the probe dye fluorescence signal constant, the transition in the stage signal from an idle stage (except along the X-axis, which is programmed to scan the sample during stand-by mode to reduce the dwell time between two tracking events) to a stochastic Brownian trajectory, and the increase in probe dye fluorescence. The probe dye of an individual molecule can either bleach before the reference dye, in which case the molecule is still tracked but the probe fluorescence signal displays a single step drop (e.g. $t \sim 22\,\mathrm{s}$), or can stay active till the molecule escapes tracking (e.g., $t \sim 17\,\mathrm{s}$), for instance due to bleaching of the reference dye. Top line shows the outcome of the clustering step, which classifies time periods corresponding to: periods of idle tracking (group 0), actively tracked molecules with a bleached probe dye (group 1), or actively tracked molecules with an active probe dye (group 2). The segmentation of the continuous data into time periods is done automatically by a step finder algorithm applied to the tracking and probe dye florescence signals, the output of which is shown as black lines overlaid on the florescence traces (step finder applied to the reference and probe dye signal shown as dashed and plain line, respectively). ***Step 2****: Estimation of background (scattering and leakage from the reference dye into the probe channel) as a function of the tracking laser power.* Left: Scatter plots of the probe fluorescence intensity and the tracking laser power during individual fluorescence periods. Groups 0 and 1 are used to estimate the background scattering noise as a function of laser power (dashed line), as well as the total background in the probe channel which includes scattering noise and fluorescence leakage of the tracking dye into the probe channel (plain line). Right: time autocorrelation function of the fluorescence intensity in the probe channel for individual fluorescence periods (thin lines), color coded by group. Group averages are shown as thick lines. Group 0 events exhibit a flat correlation signal confirming that these periods do not correspond to background noise. Group 1 molecules exhibit a non-flat correlation signal, which reports on the leakage of reference dye (the only active dye for this group) into the probe channel. Oscillations at short time lag are visible and stem from the 100 kHz rotation of the tracking laser. ***Step 3****. Estimation of signal-to-noise values.* Scatter plot of the signal-to-noise factors θ_l and θ_r estimated for each molecule in group 2. ***Step 4****. Background corrected fluorescence intensities and correlation functions.* Left: Fluorescence correlation functions of individual molecules in group 2, after background correction, applied using the signal-to-noise factors evaluated in Step 3. Right: Same scatter plot as in step 2, but after background correction.

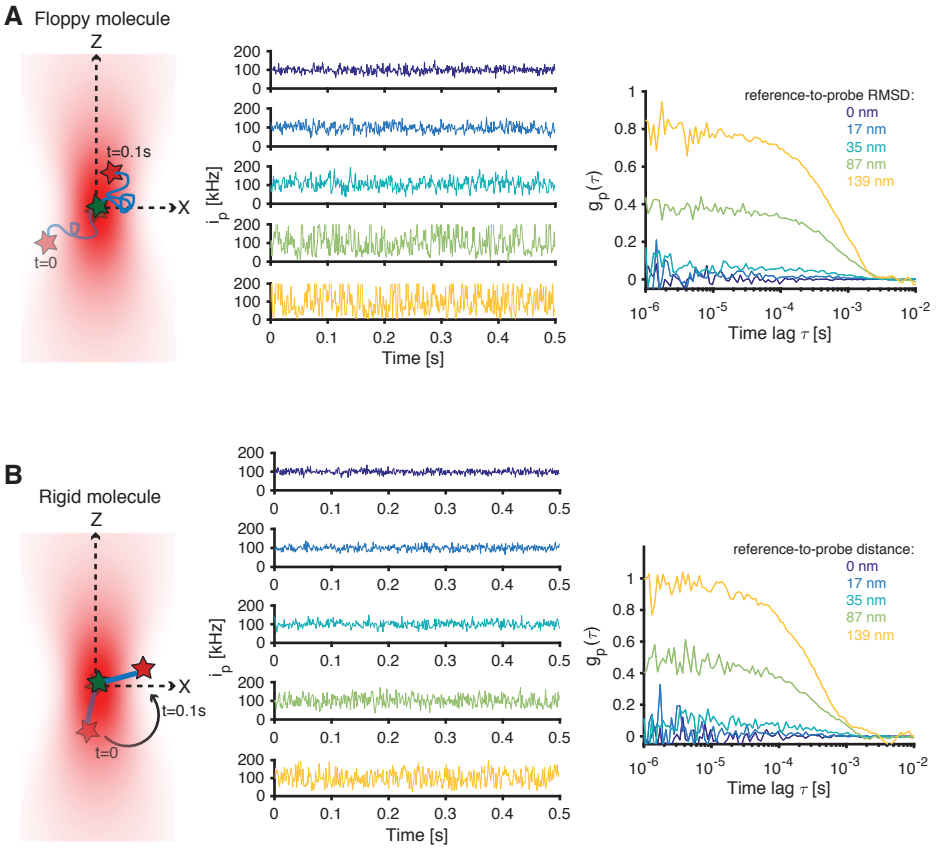

Figure S2. Readout of intramolecular distances in tFCS. Schematic of the molecular motion that generates fluorescence fluctuations and simulated tFCS data for (A) floppy molecules and (B) rigid molecules with a fixed distance between the reference and probe dyes. In both (A) and (B), the probe intensity trace $i_p(t)$ (middle panel) and the corresponding fluorescence correlation function $g_p(\tau)$ (right panel) are shown for individual molecules of various lengths. For floppy molecules, where the distance between the reference and probe dyes fluctuates, the amplitude of the intensity fluctuations and of the correlation signal encode the reference-to-probe dye root mean square distance (RMSD). For rigid molecules, the intensity fluctuations result from the rotational diffusion of the molecule about the reference dye and thus directly encode the reference-to-probe dye distance. The dynamics model used in (A) and (B) is the same as in **Fig. S4** and **Fig. S7**, respectively. Each molecule was simulated for 5 s, with 500 000 photons collected (100 000 photons/s mean fluorescence rate) and using a side-illumination geometry (probe beam waist $w = 310$ nm, probe beam offset $1.0\,w$ in (A) and $1.2\,w$ in (B)).

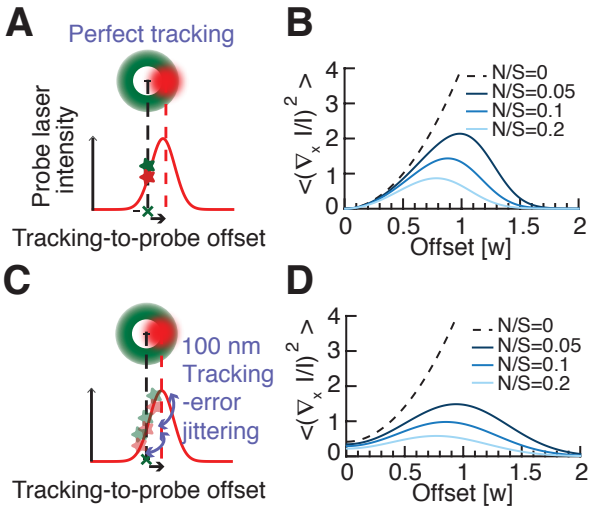

Figure S3. Heuristic spatial sensitivity of the tFCS assay. (**A**) Schematic representation of the side-illumination configuration, with tunable tracking-to-probe beam offset (same as in **Fig. 2**) (**B**) Curves show the relative intensity gradient as a function of the tracking-to-probe beam offset (in units of beam waist w) for various noise-to-signal N/S values (N is the background intensity and S is the fluorescence intensity from the probe dye placed at the focus of the beam, typical experimental value $N/S \sim 0.2$). (**C,D**) Same as in (A,B) but taking into account imperfect feedback (100 nm RMS localization error) which results in a jittering of the reference dye in the illumination profile. The jittering effectively reduces the probe laser intensity gradient seen by the probe dye.

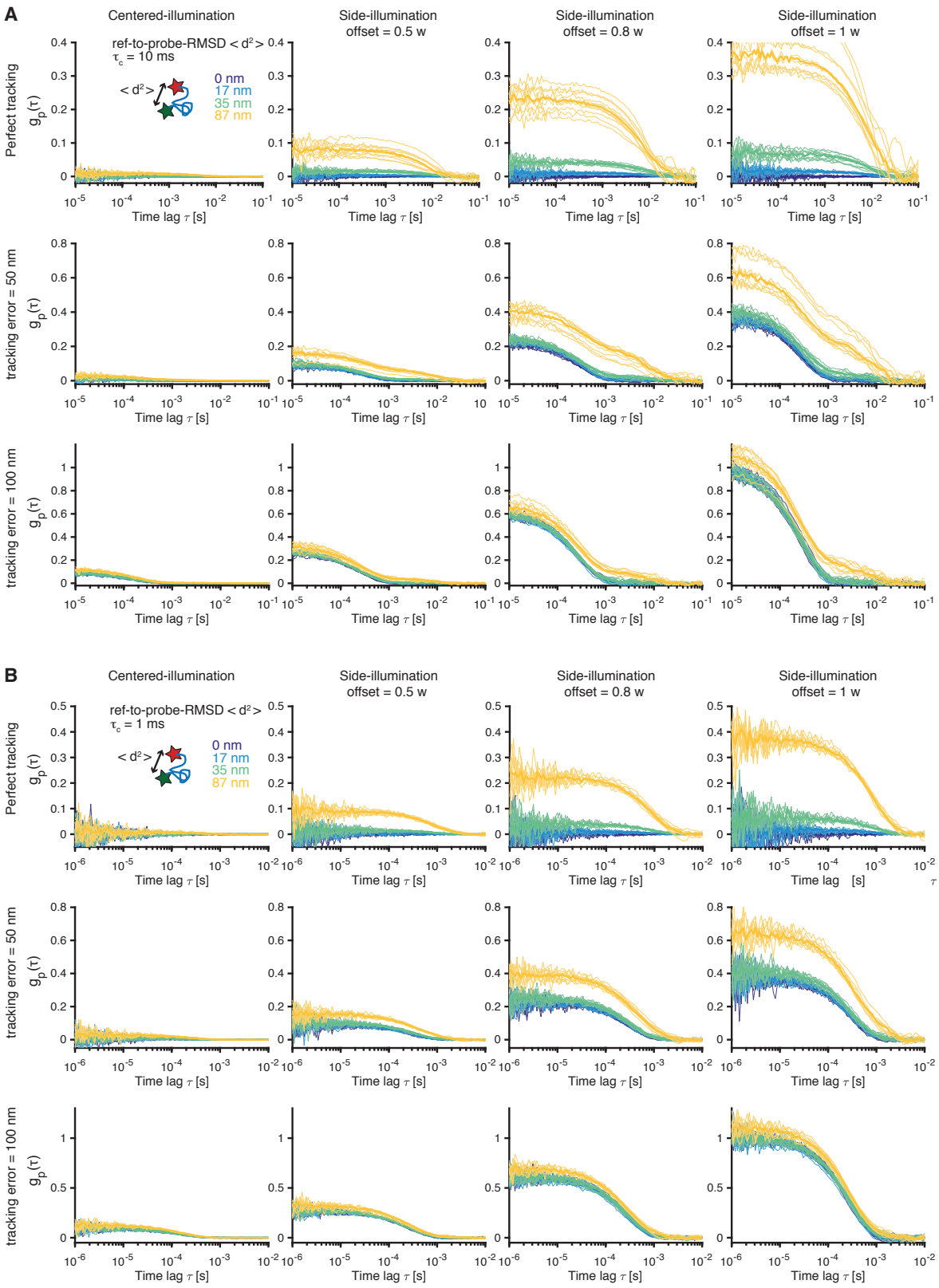

Figure S4. Spatial resolution of tFCS - numerical simulations.

Simulated tFCS signals for various illumination conditions and tracking localization errors. The reference-to-probe intramolecular dynamics was modeled as a mono-exponential relaxation (Ornstein-Uhlenbeck process) with a relaxation timescale of (**A**) 1 ms or (**B**) 10 ms, and a root mean squared distance (ref-to-probe RMSD) of 0, 17, 35 or 87 nm. $w = 310$ nm is the diffraction limited probe beam waist at the focus. For all the simulation conditions, we simulated 10 molecules for 1 s each, with a probe dye fluorescence of 10^5 photons/s and a background noise of 10^4 photons/s. Plots from row 1, columns 1 and 4, and from row 4, column 4 in (A) are replotted from Fig. 2 for completeness, but show the signal of individual molecules rather that the mean ($\pm$95% CI) tFCS signal averaged across all the molecules.

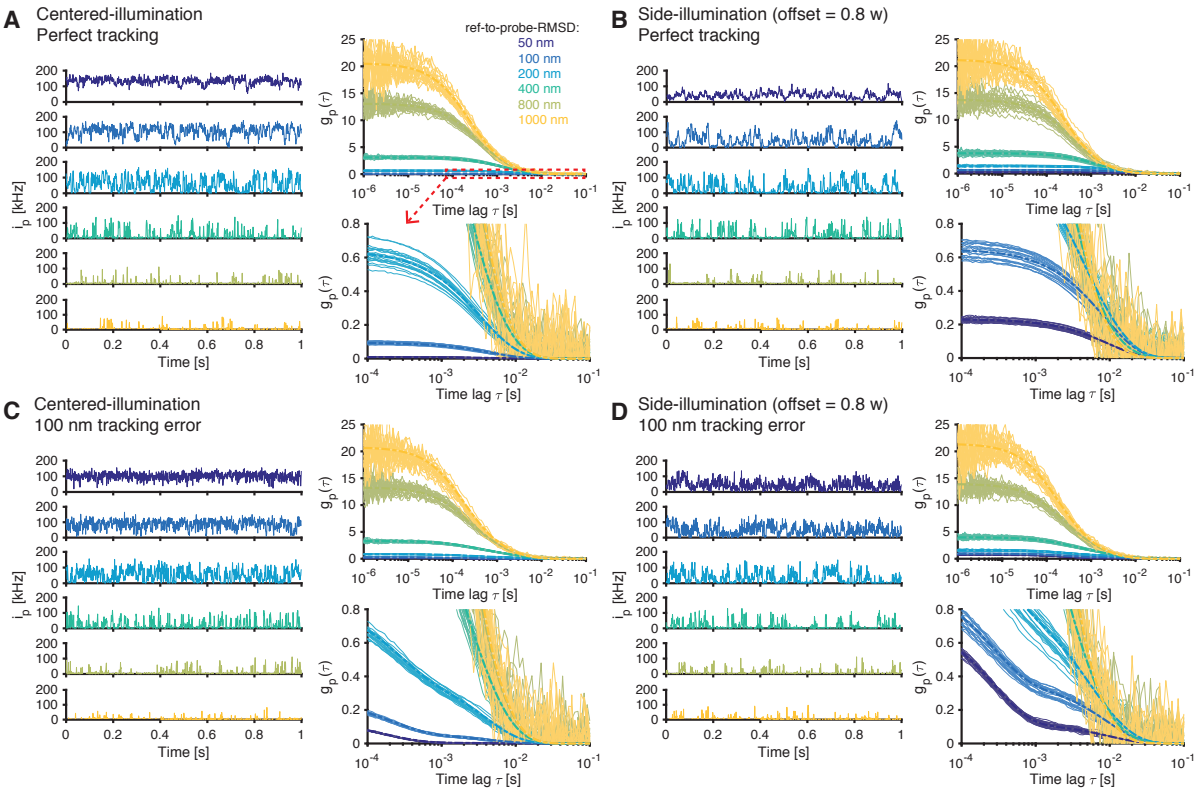

Figure S5. Intramolecular dynamics of large molecules - numerical simulations. Simulated tFCS data of molecules with a reference-to-probe dye root mean squared distance (ref-to-probe RMSD) of 50, 100, 200, 400, 800 and 1000 nm, showing that tFCS can resolve intramolecular dynamics at these length scales. The reference-to-probe dye dynamics was modeled as a mono-exponential relaxation (Ornstein-Uhlenbeck process) with a relaxation timescale of 10 ms. Simulations where done using the centered-illumination geometry (A and C) and side-illumination geometry (B and D, offset $1.0\,w$, where $w = 310$ nm), and with either perfect tracking (A and B), or 100 nm tracking localization error (C and D). For all four conditions, we simulated 10 molecules for 5 s each, with a probe dye fluorescence of 10^5 photons/s at the center of the probe beam, and a background noise of 2×10^4 photons/s (signal/noise = 5). In (A-D), the first 1 s of the probe intensity trace of a random molecule (left panel) and the fluorescence correlation signal of each individual molecule (top right panel, and zoom in on the shorter molecules at the bottom right) are shown. In all the simulations, the axial variation of the probe beam intensity was ignored to facilitate comparison between the simulated data and the theoretical predictions (dashed lines, Eq. 35). All the intensity traces and fluorescence correlation signals were background corrected (Eq. 17).

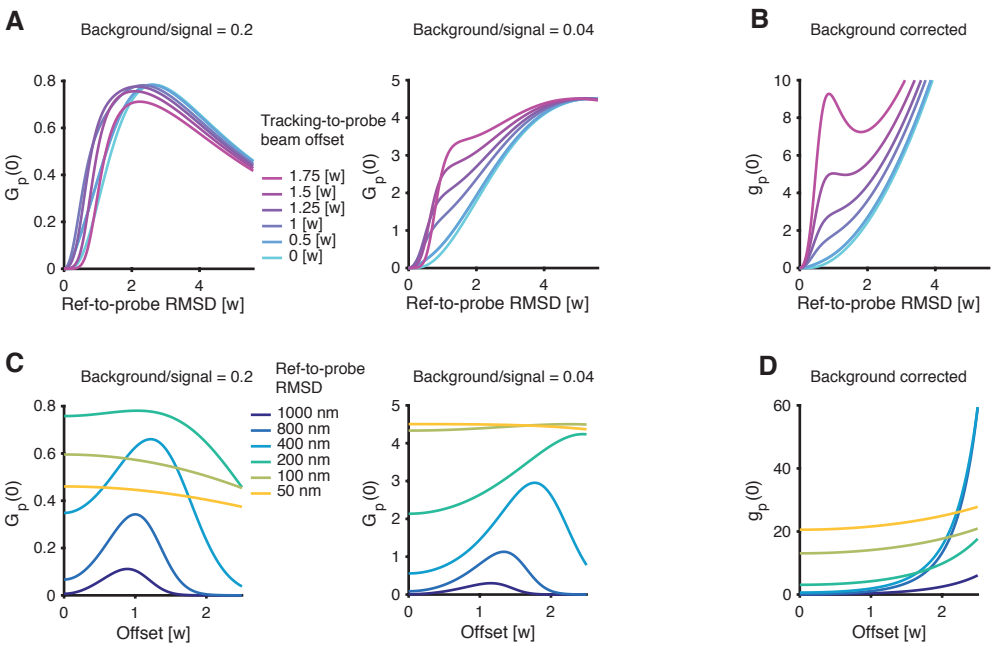

Figure S6. Amplitude of the tFCS signals as a function of the reference-to-probe fluctuation amplitude and the illumination offset. (A) Predicted amplitude of the raw fluorescence correlation signal $G_p(0)$ as a function the RMS amplitude of the reference-to-probe dye dynamics. Background/signal is defined as the ratio of the background intensity to the fluorescence intensity from the dye when it is located at the center of the probe laser. **(B)** Predicted amplitude of the fluorescence correlation signal $g_p(0)$ after background correction. These theoretical curves come from Eq. 35 and assume that the probe dye dynamics is isotropic with independent motions along the x, y, z axes. Blinking of the dye is ignored. **(C-D)** Predicted correlation amplitudes as in (A-B), but as a function of the tracking-to-probe beam offset. $[w]$ indicates that the length units are normalized with respect to the beam waist.

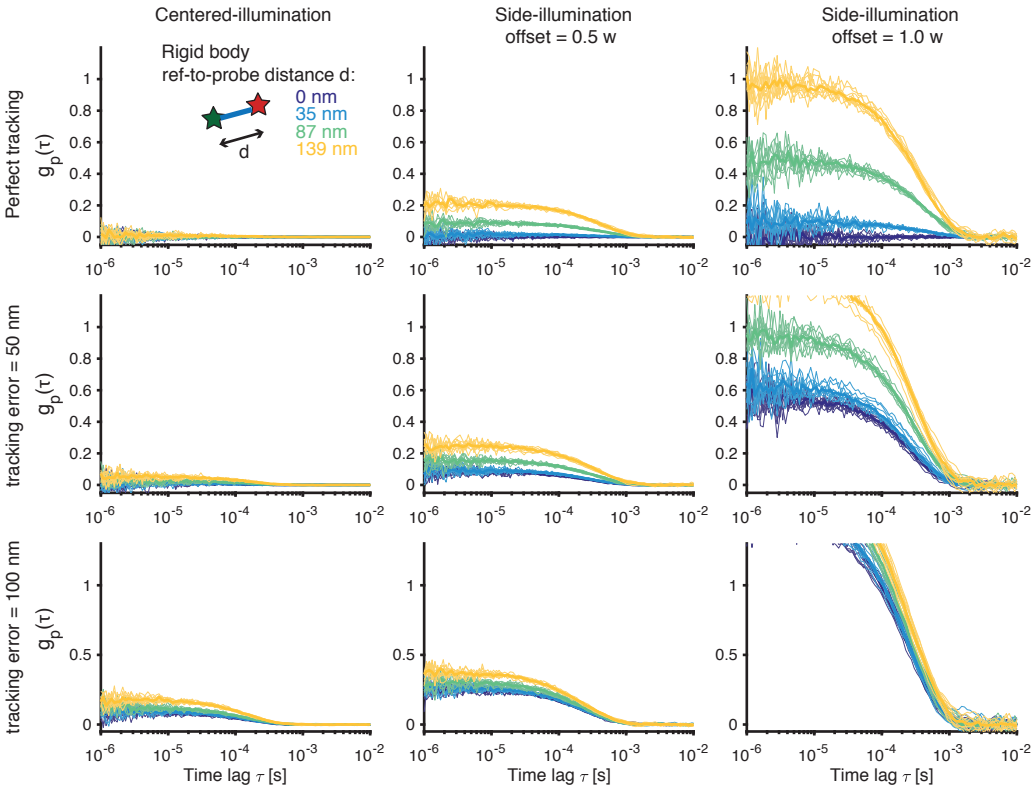

Figure S7. Spatial resolution of tFCS for measuring static distances – numerical simulation. Simulated tFCS signals of rigid molecules with a reference-to-probe dye distance of 0, 35, 87 or 139 nm, resulting from their rotational diffusion around the reference dye (the molecular tumbling is not constrained by the tracking feedback). We assumed a rotational diffusion timescale of 10 ms. For all of the simulation conditions, we simulated 10 molecules for 5 s each, with a probe dye fluorescence of 10^5 photons/s and a background noise of 10^4 photons/s. All of the intensity traces and fluorescence correlation signals were background corrected (Appendix, Eq. 17). Signals from individual molecules (thin lines) and population average (thick lines) are shown.

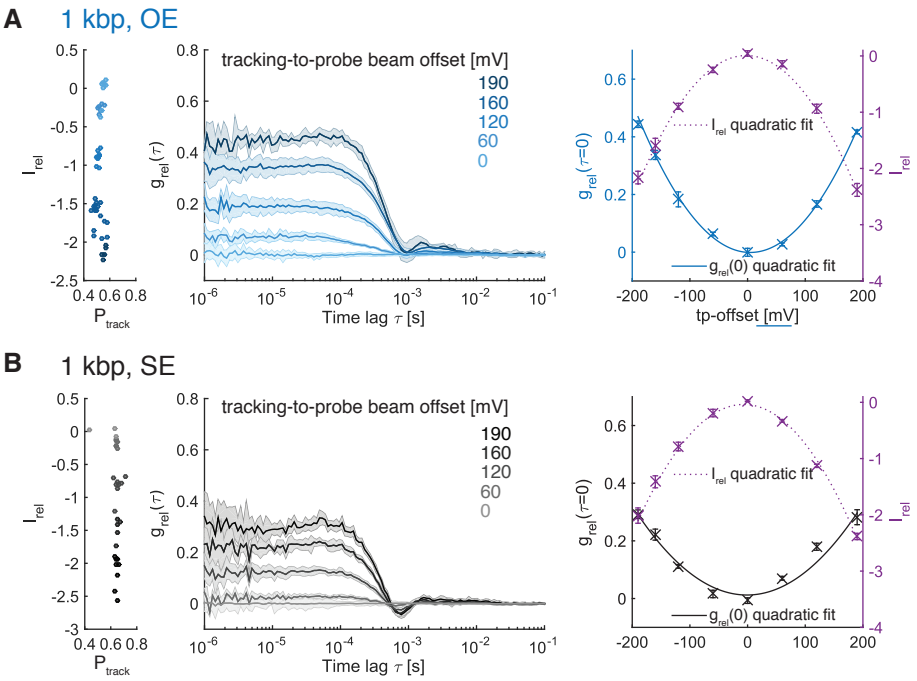

Figure S8. Effect of the tracking-to-probe beam offset on the relative fluorescence correlation functions. (**A**) Left: scatter plot of the relative intensity values I_{rel} as a function of the tracking laser power P_{track} for individual 1 kbp OE DNA molecules, measured using different tracking-to-probe beam offsets (increasing offsets in darker shades of blue). Middle: Relative correlation functions $g_{\mathrm{rel}}(\tau)$ for the same molecules (mean $\pm$ std), same color code as in left scatter plot. The relative correlation functions and intensities are computed by subtracting the side-illumination data of individual molecules from the average correlation function and intensities, respectively, across all molecules measured with the centered-illumination, using the expression of $g_{p,\mathrm{rel}}$ and I_{rel} (**SI Material and Methods** Eqs. 39 and 42). Right: Quadratic dependency of the relative correlation function amplitude and the relative intensity on the tracking-to-probe offset, shown as a quadratic fit of the data and as predicted by Eqs. 43 and 44). Crosses are sample median $\pm\,1.4826\,$Median Absolute Deviation (MAD). (**B**) Same as in (A), but for 1 kbp SE DNA molecules.

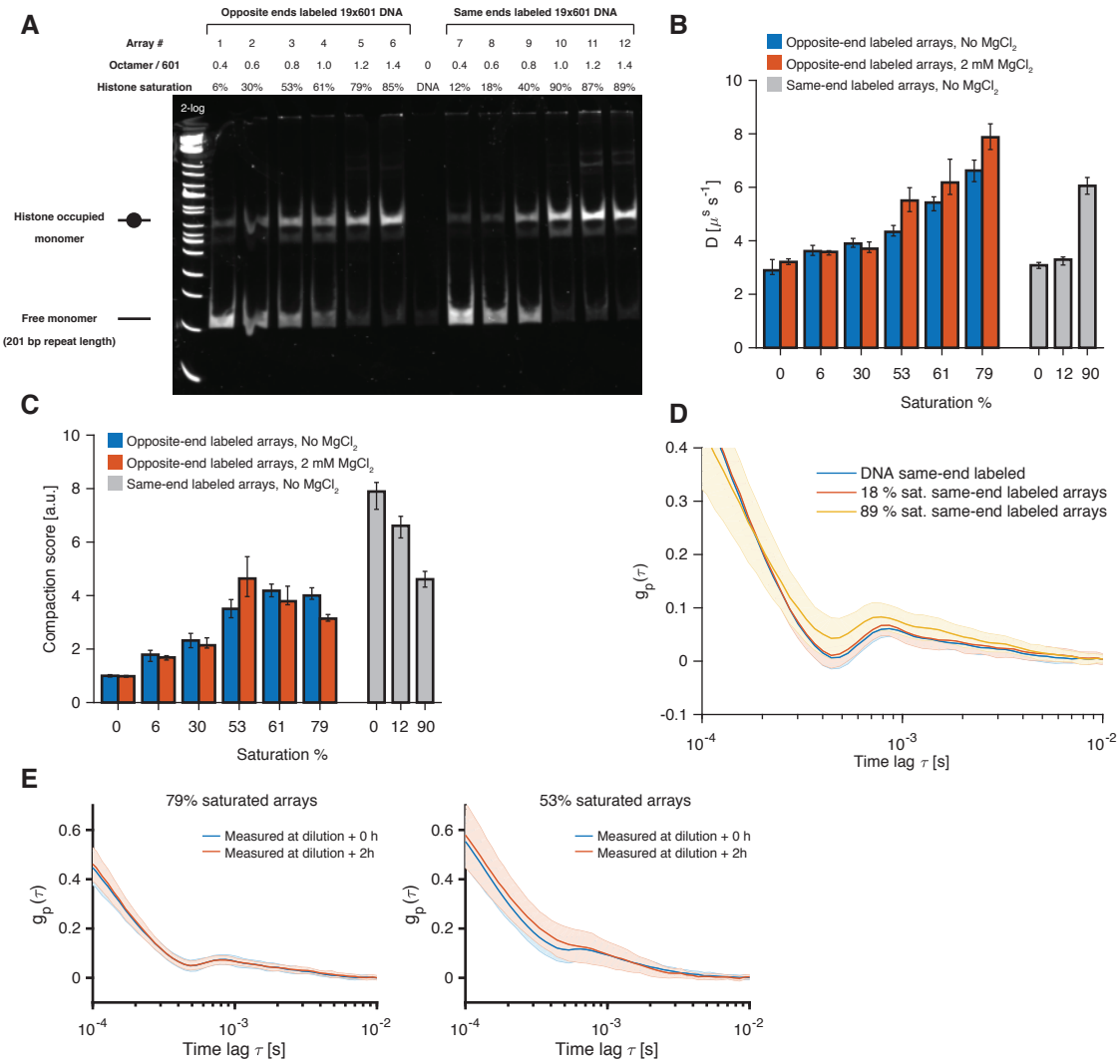

Figure S9. Characterization of nucleosome array saturation and stability, and of the tFCS noise floor for array compaction measurement. (A) Native-PAGE of nucleosome arrays after AvaI restriction digest. AvaI cuts in between each 201 bp long monomeric unit of the nucleosome positioning sequence (601 sequence). Not all arrays shown in this gel are measured by tFCS. **(B-C)** Median (±95% bootstrap confidence intervals) diffusivity (B) and compaction score (C) of DNA and nucleosome arrays. From left to right: bare DNA labeled with the reference and probe dyes on opposite ends, arrays #1-5 (labeled on opposite ends) before (blue) and after (red) addition of 2 mM magnesium, bare DNA labeled with the reference and probe dyes on the same ends, and arrays #7 and #10. Data for bare DNA and arrays are reproduced from **Fig. 4**. **(D)** tFCS signals of control DNA and arrays labeled on the same ends. The increase in tFCS amplitude and corresponding decrease in compaction score for the 79% saturated array is due to an increase in tracking error as a result of faster diffusion. **(E)** Stability of nucleosome arrays during single molecule tracking. tFCS signals (population media ± std.) of 79% and 53% saturated arrays recorded immediately after dilution to the tFCS concentration (1 pM in labeled arrays), or 2 h after dilution.

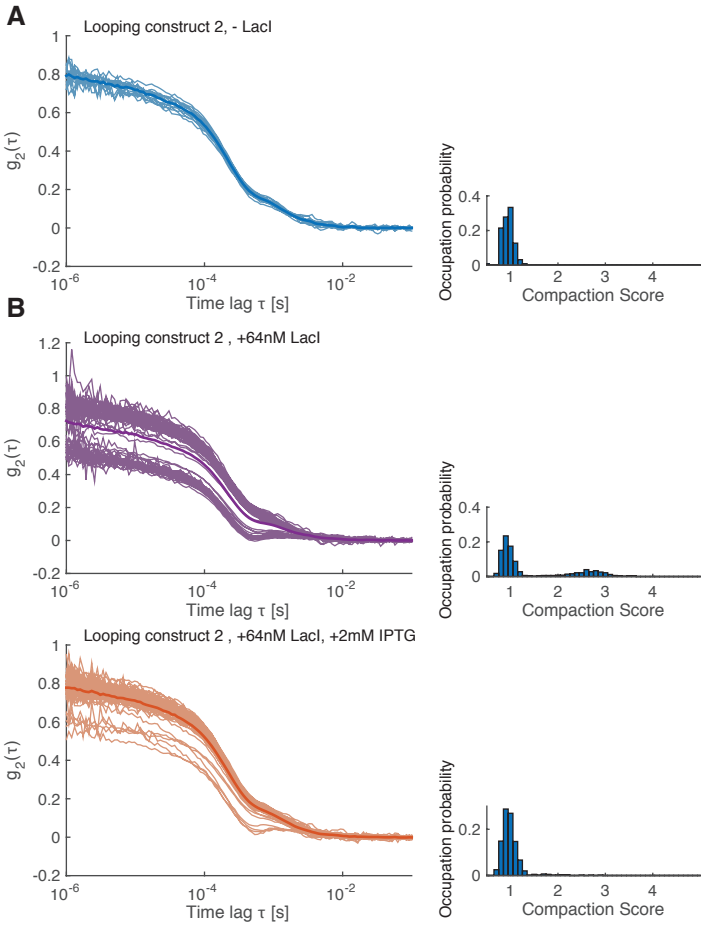

Figure S10. IPTG prevents the formation of LacI-induced DNA loops. (**A**) tFCS signals of individual DNA molecules from the looping construct 2 (**Table S1**) in absence of LacI (left) or after 5 minutes incubation with 64 nM LacI (middle), followed by addition of 2 mM IPTG (right). (**B**) Distribution of the compaction score for the three conditions in (A).

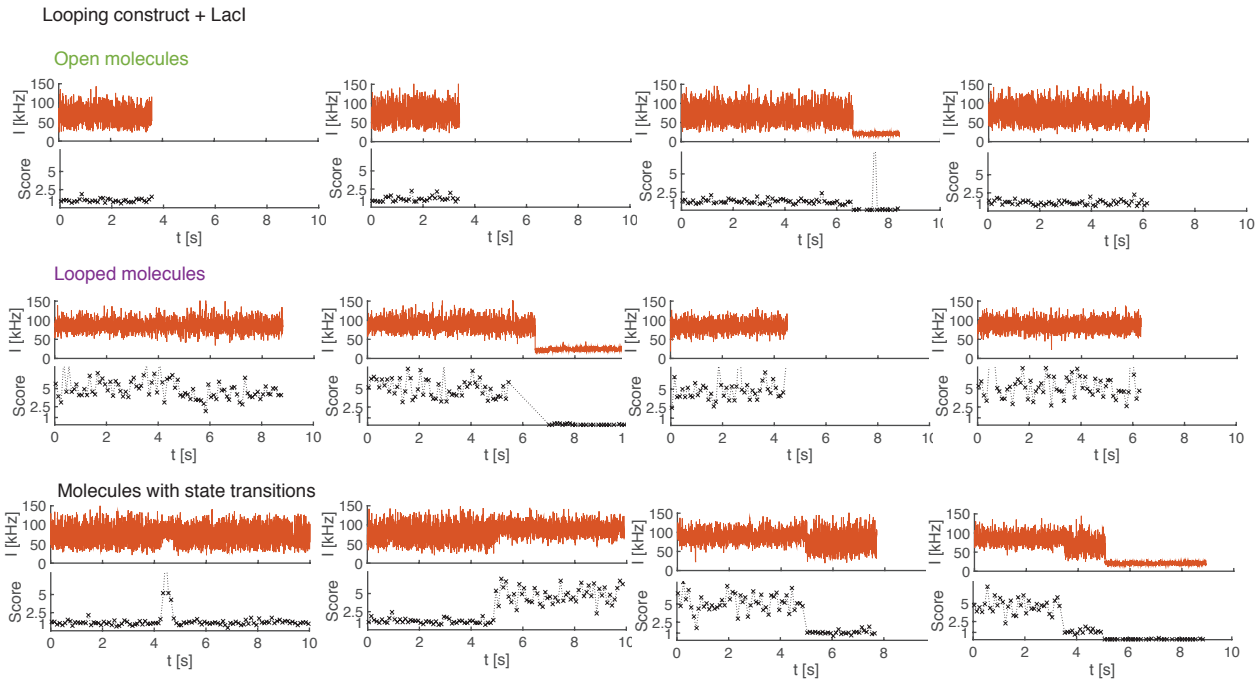

Figure S11. Examples of molecules in the looped and open conformations, and examples of transitions between the two states. Recordings of individual molecules from the looping constructs. For each molecule, the fluorescence intensity from the probe dye is shown binned at 3 ms (top plot), and the trajectory of the compaction score is shown binned at 100 ms (bottom plot).

Oligos	Sequence	Source
#118	**CTAG**AATTGT GAGCGGATAA CAATTACACC ACCATACCGT GTCTCG	IDT
#120	**AATT**AAaTGT GAGCGagTAA CAAccGTCAA GCACTGGAAC GTCGAG	IDT
#132	/5Phos/ AATTGTTATC CGCTCACAAT T	IDT
#133	/5Phos/ ggTTGTTAct CGCTCACAtT T	IDT
#140	AATTACACCA CCATACCGTG TCTCGAAaTG TGAGCGagTA ACAAccGTCA AGCACTGGAA CGTCGAG	IDT
#141	/5Phos/ GGCTGTACGT GTGGAATCAG AAGTGGCCGC GCGGCGGCAG TGCAGGCT CTAGAGCCTG CACTGCCGCC GCGCGGCCAC TTTTGAGTCC ACACTTACAA CCACACCACC	IDT
#142	ATACCGTGTC TCG	IDT
Primers	**Sequence**	**Source**
#P1	/5Biosg/ CTCGACGTTC **/iUniAmM/** CAGTGCTTGAC	IDT
#P2	CGAGACACGG **/iUniAmM /** TATGGTGGTGT	IDT
#P3	/5Biosg/ CTCGACGTTC **/iCy3b/** CAGTGCTTGAC	Labeled #P1, gel purified
#P4	CGAGACACGG **/iATTO647N /** TATGGTGGTGT	Labeled #P2, gel purified
#P5	CGAGACACGG **/iAlexa647 /** TATGGTGGTGT	Labeled #P2, gel purified
Geneblocks	**Sequence**	**Source**
Geneblock	1 CCATTCTGCC TGGGGACGTC GGAGCGATAT C**CGAGACACG GTATGGTGGT GT**GCTAGCTC 61 TCATCTCACG CAGTCCGC**AA TTGTGAGCGG ATAACAATT**G ATTGTGCGAG ACAATGCTAC 121 CTGCAGGGGC CTAGGCGGGC GAGGCTGCTC CCACCAGCAG GGGGCGCTTT GACTCGCATG 181 CCCTTACCGG TCGGAACTCG A**GAATTC**GGC GCGCCGACAG ATCTCTGGAG AATCCCGGTG 241 CCGAGGCCGC TCAATTGGTC GTAGCAAGCT CTAGCACCGC TTAAACGCAC GTACGCGCTG 301 TCCCCCGCGT TTTAACCGCC AAGGGGATTA CTCCCTAGTC TCCAGGCACG TGTCAGATAT 361 ATACATCCTG TCCTCGAGC**T CTAGA**CGCTC AGCCTCACTA CTCATACTAG TAGTCACCAC 421 TGCCGCCTCT CGGCCATTTC CGTCTCCACA GCCACAACCA AGCTTTCGGT TGAACTCTAT 481 CACGCCCATG G**AAATGTGAG CGAGTAACAA CC**GGATCCCT GGTCTTCGAA GTTAGCACAC 541 GCGT**GTCAAG CACTGGAACG TCGAG**GATAT CCCCTATAGT GAGTCGTATT ACGTAG	IDT
Capping fragments	**Sequence**	**Source**
Cap1	Anneal : #118 + #132 + #P4	Annealed
Cap2	Anneal : #120 + #130 + #P3	Annealed
Cap3	Anneal : #140 + #133 + #P3 + #P4	Annealed
Cap4	Anneal : #141 + #142	Annealed
Cap5	Anneal : #118 + #132 + #P5	Annealed
Sequence aliases	**Sequence**	
R0	1 CGAGACACGG /iATTO647N / TATGGTGGTG T	
R5	1 CTCGACGTTC /iCy3b/ CAGTGCTTGA C	
LacO1	1 AATTGTGAGC GGATAACAAT T	
LacO2	1 AAATGTGAGC GAGTAACAAC C	
LacOsym	1 AATTGTTATC CGCTCACAAT T	
DNA constructs	**Sequence**	**Source**
0.5 kb SE	Cap 3 + (391 bp from random plasmid digestion with XbaI EcoRI) + Cap 4	Ligation + gel purification
1.0 kb SE	Cap 3 + (898 bp from random plasmid digestion with XbaI EcoRI) + Cap 4	Ligation + gel purification
3.9 kb SE	Cap 3 + (3792 bp from random plasmid digestion with XbaI EcoRI) + Cap 4	Ligation + gel purification
0.5 kb OE	Cap 1 + (391 bp from random plasmid digestion with XbaI EcoRI) + Cap 2	Ligation + gel purification
1.0 kb OE	Cap 1 + (898 bp from random plasmid digestion with XbaI EcoRI) + Cap 2	Ligation + gel purification
3.9 kb OE	Cap 1 + (3792 bp from random plasmid digestion with XbaI EcoRI) + Cap 2	Ligation + gel purification
6.1 kb OE	Cap 1 + (5992 bp from random plasmid digestion with XbaI EcoRI) + Cap 2	Ligation + gel purification
LacO looping	R0 - (20 random bp) - LacO1 - (~2600 random bp) - LacOsym - (random 32 bp) - R5'	PCR R0 and R5' primers
LacO lasso	R0 - (20 random bp) - LacO1 - (~1300 random bp) - LacO1 - (~random 1300 bp) - R5'	PCR R0 and R5' primers
LacO 3 sites	R0 - (20 random bp) - LacO1 - (~1300 random bp) - LacO1 - (~random 1300 bp) - LacOsym - (random 32 bp) -	PCR R0 and R5' primers
LacO looping 2	R0 - (20 random bp) - LacO1 - (2608 random bp) - LacO2 - (random 32 bp) - R5'	PCR R0 and R5' primers
19x601 kb for	Cap 5 + (19x601 array with XbaI EcoRI overhangs) + Cap 2	Ligation + gel

Prime (') indicates reverse complement

Table S1. DNA constructs and oligonucleotides used in this study.

Experiment #1	DNA end-to-end dynamics						
Illumination conditions	Centered-illumination, Side-Illumination						
Detector config.	P/P						
Dyes	Cy3b, Atto647 N						
Sample	**# mol. group 2**	**# included**	**median(T) [s]**	**std(T) [s]**	**max(T) [s]**	**median(Nphotons)**	**std(Nphotons)**
487 OE, centered illum.	17	15	3.5	2.0	13.1	459759.0	206.3
994 OE, centered illum.	8	8	3.4	1.0	9.0	438878.0	180.8
3888 OE, centered illum.	5	3	4.0	3.1	6.1	387648.0	293.7
487 SE, centered illum.	27	27	2.8	1.5	13.2	347900.0	174.7
994 SE, centered illum.	3	3	2.5	1.3	3.4	365077.0	199.3
3888 SE, centered illum.	10	8	4.1	3.5	13.2	633710.0	554.5
487 OE, centered illum.	17	15	2.8	1.1	9.9	159709.0	60.2
994 OE, side illum.	18	15	4.1	2.6	8.3	239249.0	143.3
3888 OE, side illum.	9	8	8.8	6.5	14.2	504698.0	385.9
487 SE, side illum.	25	19	3.7	3.1	10.2	206416.0	176.8
994 SE, side illum.	6	5	2.2	1.5	8.7	148137.0	113.7
3888 SE, side illum.	13	11	4.8	5.0	10.4	353416.0	373.4
Experiment #2	**Nucleosome arrays**						
Illumination conditions	Side-Illumination						
Detector config.	R/P						
Dyes	Cy3b, Alexa647						
Sample	**# mol. group 2**	**# included**	**median(T) [s]**	**std(T) [s]**	**max(T) [s]**	**median(Nphotons)**	**std(Nphotons)**
19x601 DNA	34	32	1.98	1.11	6.20	78998.0	45742.00
19x601 DNA +2mM Mg	55	47.00	3.08	1.76	9.69	138900.0	86216
Arrays 6% saturation	82	68.00	2.02	1.41	9.65	86103.0	56038
Arrays 6% saturation +2mM Mg	120	100.00	2.75	1.69	12.52	126140.0	75604
Arrays 30% saturation	81	70.00	1.56	0.73	4.01	57540.0	28062
Arrays 30% saturation +2mM Mg	71	56.00	2.53	1.71	20.52	122190.0	94445
Arrays 53% saturation	98	83.00	1.78	1.21	8.85	85243.0	59737
Arrays 53% saturation +2mM Mg	15	11.00	3.10	2.24	5.83	115250.0	104480
Arrays 61% saturation	62	51.00	1.51	1.03	6.38	62519.0	41064
Arrays 61% saturation +2mM Mg	26	20.00	2.44	1.74	6.86	129170.0	95436
Arrays 79% saturation	53	44.00	2.30	1.68	7.38	87780.0	71750
Arrays 79% saturation +2mM Mg	64	52.00	2.83	2.46	10.21	141130.0	129190
19x601 DNA same-end labeling	85	68.00	2.19	1.17	11.15	92625.0	62383
Arrays same-end 18% saturation	94	86.00	1.71	0.81	8.41	67040.0	30977
Arrays same-end 90% saturation	91	76.00	1.59	0.84	7.67	76134.0	40472
Experiment #3	**LacI induced looping**						
Illumination conditions	Side-Illumination						
Detector config.	R/P						
Dyes	Cy3b, Atto647 N						
Sample	**# mol. group 2**	**# included**	**median(T) [s]**	**std(T) [s]**	**max(T) [s]**	**median(Nphotons)**	**std(Nphotons)**
2.5 kb SE	31	29	2.8	1.4	9.9	212208.0	116222.0
LacO Looping -LacI	8	7	4.1	1.8	9.2	216523.0	90544.7
LacO Looping +LacI	61	61	3.5	2.6	15.3	193024.1	170208.5
LacO Lasso +LacI	64	64	3.1	2.3	16.5	171235.0	123537.9
LacO 3 sites +LacI	32	32	2.6	1.8	9.8	164863.3	129426.1
LacO Looping 2 - LacI	14	14	2.8	1.1	14.2	206329.4	101200.1
LacO Looping 2 +LacI	65	65	3.2	2.2	13.3	225997.9	150074.2
LacO Looping 2 +LacI +IPTG	59	59	4.1	2.9	24.4	306211.2	248106.0

Table S2. Experimental conditions and tracking statistics.